



# A consistent strain-based beam element with quaternion representation of rotations

Damjan Lolić<sup>1</sup> · Dejan Zupan<sup>2</sup> · Miha Brojan<sup>1</sup>

Received: 7 November 2019 / Accepted: 3 February 2020 / Published online: 10 February 2020  
© Springer-Verlag GmbH Germany, part of Springer Nature 2020

## Abstract

We present a novel consistent singularity-free strain-based finite element formulation for the analysis of three-dimensional frame-like structures. Our model is based on a geometrically exact finite-strain beam theory, quaternion parametrization of spatial rotations, assumption that the strain measures are constant along the length of the element and a proper choice of basis for the translational strain vector representation. As it is common for strain-based elements, the present formulation does not suffer from shear locking. A comparison of our results with the results from the literature and a commercial finite element analysis software demonstrates the advantages of the proposed formulation, especially when the structure is subjected to larger shear deformations. This stems from the fact that our model ensures a mathematically consistent updating procedure for all the quantities describing the beam. This aspect is often overlooked, since most of the numerical cases from other studies on this topic engage rather small-shear strains for which the consistent update is not crucial as the number of elements is increased.

**Keywords** Three-dimensional Reissner beam · Rotational quaternion · Strain vector · Global basis

## 1 Introduction

Nonlinear spatial beam theory is indispensable in many different fields of science; ranging from structural engineering [1,2], microbiology [3], nanotechnology [4], computer graphics [5,6] to photogrammetry [7] and robotics [8]. Under various constraints and theoretical assumptions, the problems from these diverse fields demand advanced formulations solution procedures to effectively solve them. Beam formulations differ in the way the kinematics of a beam-like structure is approximated. An important milestone in the evolution of the beam models is the geometrically exact theory of plane beams by Reissner [9] as it represents the beginning

of the revival of research on this topic. Succeeding the classical Cosserat beam theory [10], Reissner [11] and Simo [12] developed exact kinematic relations between displacements and deformations for a spatial beam through the use of virtual work principle without the constraints on the magnitudes of strains, internal forces, displacements and rotations. Later, Simo and Vu-Quoc [13] presented numerical implementation of the theory using the finite element method. These classical works have motivated many other researchers developing the modern beam finite element formulations, see e.g. Cardona and Géradin [14], Ibrahimbegović [15], Jelenić and Saje [16], Smolénski [17], etc.

We can classify beam formulations according to: the kinematic assumptions used, how the rotations are parametrized and which variables are chosen as primary. Rotations are often a member of the primary variables in three-dimensional beam formulations, even though they require a special treatment. Several mathematical models to describe rotations have been proposed, such as Euler angles, rotation matrix, rotational vector, direction cosine matrix, rotational quaternion, etc., see e.g. Argyris [18], Argyris and Poterasu [19], Géradin and Rixen [20], Spring [21], Atluri and Cazzani [22], Zupan et al. [23]. Among them, the rotational vector is often preferable over other parametrizations of rotations because

✉ Miha Brojan  
miha.brojan@fs.uni-lj.si

Damjan Lolić  
damjan.lolic@fs.uni-lj.si

Dejan Zupan  
dejan.zupan@fgg.uni-lj.si

<sup>1</sup> Faculty of Mechanical Engineering, University of Ljubljana, Askerceva 6, 1000 Ljubljana, Slovenia

<sup>2</sup> Faculty of Civil and Geodetic Engineering, University of Ljubljana, Jamova 2, 1000 Ljubljana, Slovenia

the rotation axis and the angle of rotation can be compacted into only three parameters (see also [13–17,24,25]). But utilizing minimal number of parameters to describe rotations may result in singular points, as shown by Stuelpnagel [26] and Atluri [22]. However, singularities can be avoided by using updated-Lagrangian schemes where the incremental rotations are interpolated and not total rotations, as seen e.g. in [27,28]. A detailed comparative analysis of these models can be found in [20–22,29]. They identify and evaluate the most important aspects, such as number of parameters needed, programming simplicity, reliability, comprehensibility, etc. Since rotational vectors are non-additive quantities, a special interpolation of rotations has to be used. Crisfield and Jelenić [30] outlined that using standard rotational-vector based formulations usually leads to non-objectivity and path-dependency. Ibrahimbegović [29] presented the shortcomings of total rotational vector when describing rotations greater than  $2\pi$ . On the other hand, incremental rotational vector [29] and orthogonal tensor representation of finite rotations [13] as upgrades are proven to give correct results even for large rotations. The same conclusions were obtained by Battini and Pacoste [31] with their co-rotational beam elements employing incremental rotational vectors. Furthermore, it appears that using four parameters (which inherently increases the number of degrees of freedom) avoids the singularity and increases computational efficiency, as shown by McRobie and Lasenby [32] in their rod formulation based on Clifford algebra. Further studies by Zupan et al. [33–35] show that using rotational quaternions, more efficient, stable and robust numerical formulations of beams for dynamic analysis can be obtained.

The resultant strains in the geometrically exact beam model can be treated as additive. With this in mind, many authors e.g. Tabarrok et al. [36], Češarek et al. [24], Zupan and Saje [25,37] interpolate strain measures. Such choice of primary variables leads to a straightforward proof of objectivity and invariance of rigid-body motion. Considering the physical nature of strain measures, they are expressed in material basis to fit into constitutive equations.

In this contribution, we formulate a strain-based finite element for the analysis of three-dimensional beams. We allow the beam to deform by flexure, torsion, extension, and shear without any restrictions on the magnitudes of displacements and rotations. The computational model is based on the geometrically exact beam theory and structured to be consistent and mathematically accurate. To ensure a singularity-free formulation, we adopt quaternion algebra to parametrize spatial rotations and employ coordinate system transformations. Strain measures are chosen here as the primary unknowns, while their additive nature is preserved using the correct choice of bases. We use a local basis for rotational strain vector  $\boldsymbol{\kappa}$  and a global (fixed) basis for the translational strain vector  $\boldsymbol{\gamma}$ . Although our choice for the component description

of translational strain vector is different than in conventional strain-based numerical models, we prove that it ensures mathematically consistent update procedure. Moreover, the strain vectors are assumed constant along the length of the beam in order to analytically integrate kinematic equations and avoid the need for any additional approximation or source of error. The influence of the chosen description of transverse strains is carefully analysed and tested with a variety of numerical examples. These include a thick cantilever beam, shear loaded double asymmetric tapered beam, a right-angle cantilever and a beam bent into a helical form. All examples are also modeled with a commercial finite element analysis software and compared to our results. The final section summarizes the work done in this study.

## 2 Theoretical formulation

In this section we present the components needed to develop the formulation. We apply quaternion algebra to describe spatial rotations, most suitable component description and variational formalism to express the strain measures. Combined with equilibrium and constitutive relations, we structure a set of governing equations, which we later solve numerically.

### 2.1 Parametrization of rotations

We choose Euler-Rodrigues parameters in a form of unit quaternions for parametrization of rotations and give a brief summary of the most important ingredients. (For a detailed review on quaternion algebra and its applications see e.g. Ward [38] and Zupan et al. [23].) We will denote quaternions with a hat symbol  $\hat{\cdot}$  and the quaternion multiplication with a symbol  $\circ$ . As spatial vectors and scalars form the subspace in the space of quaternions, the rules of vector and scalar algebra also apply in quaternion manipulation.

A quaternion  $\hat{a}$  is a combination of a scalar and a vector, formally presented as:

$$\hat{a} = a_0 + \mathbf{a}, \quad a_0 \in \mathbb{R}, \quad \mathbf{a} \in \mathbb{R}^3, \quad (1)$$

with the norm  $|\hat{a}| = \sqrt{a_0^2 + |\mathbf{a}|^2}$ , where  $|\mathbf{a}| = \sqrt{\mathbf{a} \cdot \mathbf{a}}$ . Its conjugated form is  $\hat{a}^* = a_0 - \mathbf{a}$ . The quaternion multiplication is associative, distributive and non-commutative; and is defined as

$$\hat{a} \circ \hat{b} = (a_0 b_0 - \mathbf{a} \cdot \mathbf{b}) + (b_0 \mathbf{a} + a_0 \mathbf{b} + \mathbf{a} \times \mathbf{b}), \quad (2)$$

where  $\cdot$  denotes the scalar product and  $\times$  the cross product. A rotational quaternion  $\hat{q} = q_0 + \mathbf{q}$  has a unit norm  $|\hat{q}| = 1$ . Moreover,

$$\hat{q} \circ \hat{q}^* = \hat{1}. \quad (3)$$

Due to the non-commutative nature of the quaternion, it is convenient to introduce two linear operators for left and right multiplication of unit quaternion  $\hat{q}$  with an arbitrary quaternion  $\hat{x}$ :

$$\hat{q} \circ \hat{x} = \phi_L(\hat{q})\hat{x}, \tag{4}$$

$$\hat{x} \circ \hat{q} = \phi_R(\hat{q})\hat{x}, \tag{5}$$

where

$$[\phi_L(\hat{q})] = \begin{bmatrix} q_0 & -q_1 & -q_2 & -q_3 \\ q_1 & q_0 & -q_3 & q_2 \\ q_2 & q_3 & q_0 & -q_1 \\ q_3 & -q_2 & q_1 & q_0 \end{bmatrix},$$

$$[\phi_R(\hat{q})] = \begin{bmatrix} q_0 & -q_1 & -q_2 & -q_3 \\ q_1 & q_0 & q_3 & -q_2 \\ q_2 & -q_3 & q_0 & q_1 \\ q_3 & q_2 & -q_1 & q_0 \end{bmatrix},$$

with  $[\hat{q}] = [q_0, q_1, q_2, q_3]^T$  and  $[\hat{x}] = [x_0, x_1, x_2, x_3]^T$  representing a component one-column form of quaternions  $\hat{q}$  and  $\hat{x}$ . When  $\hat{q}$  has a unit norm,  $\phi_L(\hat{q})$  and  $\phi_R(\hat{q})$  are orthogonal; thus  $\phi_L(\hat{q})^T = \phi_R(\hat{q})$  and  $\phi_R(\hat{q})^T = \phi_L(\hat{q})$ . Therefore operators  $\phi_L$  and  $\phi_R$  represent rotations in four-dimensional space as they conserve the length, the angle and the orientation of  $\hat{x}$ . But in the case of three-dimensional rotations, when vectors (pure quaternions) are involved, operators  $\phi_L$  and  $\phi_R$  do not map pure quaternions (vectors) into pure quaternions. Consequently, an appropriate combination of two operators that preserves the length of the mapped vector in  $\mathbb{R}^3$  has to be defined. A combination of two consecutive rotations is again a rotation [38]. Here, a left and right quaternion multiplication is used to construct operator  $Q$  as follows

$$\hat{q} \circ \hat{x} \circ \hat{q}^* = Q(\hat{q})\hat{x}, \tag{6}$$

$$Q(\hat{q}) = \phi_L(\hat{q})\phi_R(\hat{q}^*) = \phi_R(\hat{q}^*)\phi_L(\hat{q}), \tag{7}$$

which reads in matrix notation:

$$[Q] = \begin{bmatrix} 1 & 0_{1 \times 3} \\ 0_{3 \times 1} & R \end{bmatrix}, \tag{8}$$

$$[R] = 2 \begin{bmatrix} q_0^2 + q_1^2 - \frac{1}{2} & q_1 q_2 - q_0 q_3 & q_0 q_2 + q_1 q_3 \\ q_1 q_2 + q_0 q_3 & q_0^2 + q_2^2 - \frac{1}{2} & -q_0 q_1 + q_2 q_3 \\ -q_0 q_2 + q_1 q_3 & q_1 q_0 + q_2 q_3 & q_0^2 + q_3^2 - \frac{1}{2} \end{bmatrix}. \tag{9}$$

Here,  $[R]$  denotes a submatrix that is often found in the literature (see e.g. Argyris [18]) and is called a standard rotation matrix in three-dimensional rotation space. It has to be mentioned that each of  $\phi_R(\hat{q}^*)$  and  $\phi_L(\hat{q})$  represent one half of the rotation. For this reason, the polar form of a quaternion representation of the rotational vector  $\vartheta$  takes the following form:

$$\hat{q} = \cos \frac{\vartheta}{2} + \mathbf{n} \sin \frac{\vartheta}{2} = \exp \left( \frac{\vartheta}{2} \right), \tag{10}$$

where  $\mathbf{n} = \vartheta/\vartheta$  is the unit vector that represents the axis of rotation and  $\vartheta$  is the angle of rotation. The rotational quaternion can also be defined with an exponential map [39]. This expression follows from the Taylor series expansion of the sine and cosine functions in Eq. (10) and reads

$$\begin{aligned} \hat{q} &= \left( 1 - \frac{1}{2!} \left( \frac{\vartheta}{2} \right)^2 + \frac{1}{4!} \left( \frac{\vartheta}{2} \right)^4 - \dots \right) \\ &\quad + \mathbf{n} \left( \frac{\vartheta}{2} - \frac{1}{3!} \left( \frac{\vartheta}{2} \right)^3 + \frac{1}{5!} \left( \frac{\vartheta}{2} \right)^5 - \dots \right) \\ &= \hat{1} + \frac{\vartheta}{2} + \frac{1}{2!} \frac{\vartheta}{2} \circ \frac{\vartheta}{2} + \frac{1}{3!} \frac{\vartheta}{2} \circ \frac{\vartheta}{2} \circ \frac{\vartheta}{2} + \dots \\ &= \exp \left( \frac{\vartheta}{2} \right). \end{aligned} \tag{11}$$

### 2.2 Geometry, kinematics

Let  $g = \{g_1, g_2, g_3\}$  denote a set of fixed orthonormal vectors, here called the global basis. A material curve  $\mathcal{L}^0$  is defined by a vector function  $\mathbf{r}_g^0$  to each point  $s$  on the material curve with respect to the origin of the coordinate system  $\mathcal{O}$ . Here,  $s$  represents the arc-length parameter of the undeformed curve. If the beam is of initial length  $L$ , then  $s \in [0, L]$ . Furthermore, let  $\mathcal{L}^0$  connect the centroids of the beam’s cross-sections and let the tangent to the curve define their orientation of the undeformed configuration of the beam (see Fig. 1). Then a local orthonormal basis  $G^0 = \{G_1^0, G_2^0, G_3^0\}$  can be defined such that the base vector  $G_1^0(s) = d\mathbf{r}_g^0(s)/ds$  is normal to the cross-section, and  $G_2^0$  and  $G_3^0$  are vectors directed along the principal axes of the second moment of area of the cross-section. Obviously,  $G_2^0 \times G_3^0 = G_1^0$ . As the coordinate system defined by  $G^0$  follows the material curve  $\mathcal{L}^0$ , we call  $G^0$  a material base. Vector  $G_1^0(s)$  is in general tangent to material curve  $\mathcal{L}^0$  only when the initial configuration is undeformed.

The deformed configuration of the beam is described in a similar manner with  $\mathbf{r}_g(s)$ ,  $G_1(s)$ ,  $G_2(s)$  and  $G_3(s)$ . As the shear strains are allowed, vector  $G_1(s)$  is not necessary tangent to the material curve  $\mathcal{L}$ . We additionally assume that the deformed cross-sections remain planar and have the same shapes and areas as in the initial configuration.

In order to apply quaternion algebra to the formulation, mathematical configuration space is expanded into four-dimensions. Every vector from the three-dimensional space is expanded with a zero scalar part to form a pure quaternion. A unit quaternion  $\hat{1}$  is also introduced to supplement the three base vectors. Local and global bases now consist of four quaternions  $\hat{G}_0, \hat{G}_1, \hat{G}_2, \hat{G}_3$  and  $\hat{g}_0, \hat{g}_1, \hat{g}_2, \hat{g}_3$ , respectively. Here  $\hat{G}_0 = \hat{g}_0 = 1 + \mathbf{0} = \hat{1}$  and  $\hat{G}_i = 0 + G_i$ ,

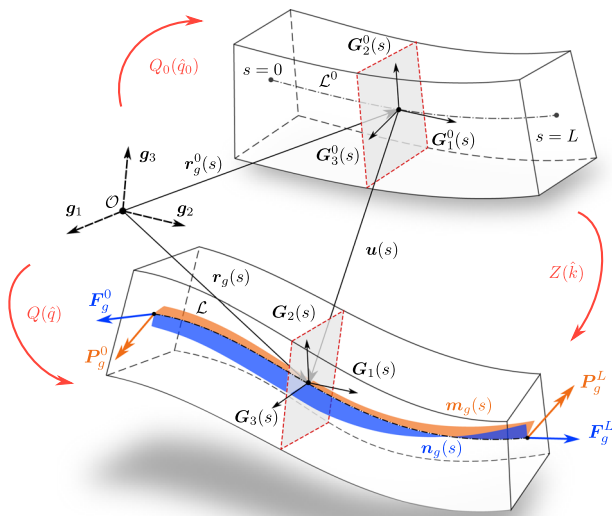


**Fig. 1** Model of a spatial beam in initial and deformed configuration. Fixed, local initial and local deformed bases are related via transformation matrices  $Q_0(\hat{q}_0)$ ,  $Z(\hat{k})$  and  $Q(\hat{q})$

$\hat{g}_i = 0 + \mathbf{g}_i$ , for  $i \in \{1, 2, 3\}$ . A spatial rotation, as well as the coordinate transformation can be obtained by the linear operator  $Q$ . Both, fixed and moving bases are thus associated via relation

$$\hat{G}_i = Q\hat{g}_i = \hat{q} \circ \hat{g}_i \circ \hat{q}^*, \quad i \in \{1, 2, 3\}. \tag{12}$$

The total rotation can be separated into an initial rotation and a relative rotation, which is in quaternion notation expressed as:

$$\hat{q}(s) = \hat{k}(s) \circ \hat{q}_0(s). \tag{13}$$

Here, the rotational quaternion  $\hat{q}_0$  represents the transformation between the global  $\mathbf{g}_i$  and local  $\mathbf{G}_i^0$  basis, while the rotational change from the initial to the deformed configuration is described by rotational quaternion  $\hat{k}$ . The rotation matrix  $Q$  is similarly replaced by a product of rotation matrices:  $Q = ZQ_0$ , where  $Z(\hat{k}) = \phi_L(\hat{k})\phi_R(\hat{k}^*)$  and  $Q_0(\hat{q}_0) = \phi_L(\hat{q}_0)\phi_R(\hat{q}_0^*)$ .

An arbitrary pure quaternion  $\hat{a}$  can be expressed in global  $[\hat{a}]_g = [0, a_{g1}, a_{g2}, a_{g3}]^T$  or local  $[\hat{a}]_G = [0, a_{G1}, a_{G2}, a_{G3}]^T$  basis. The transformation between both representations is obtained through rotation  $Q$ :

$$\hat{a}_g = Q\hat{a}_G = \phi_L(\hat{q})\phi_R(\hat{q}^*)\hat{a}_G = \hat{q} \circ \hat{a}_G \circ \hat{q}^*. \tag{14}$$

Since  $Q$  is orthogonal, we can also write an inverse transformation as,

$$\begin{aligned} \hat{a}_G &= Q^T \hat{a}_g = \phi_L^T(\hat{q})\phi_R^T(\hat{q}^*)\hat{a}_g = \phi_R(\hat{q})\phi_L(\hat{q}^*)\hat{a}_g \\ &= \hat{q}^* \circ \hat{a}_g \circ \hat{q}. \end{aligned} \tag{15}$$

### 2.3 Variation of rotational quantities

Three-dimensional rotations can be chosen as primary unknowns of the spatial beam. With rotations not being additive quantities, we have to look into their variation prior to the linearization process. We write the variation of Eq. (12) as follows

$$\begin{aligned} \delta \hat{G}_i &= \delta \hat{q} \circ \hat{g}_i \circ \hat{q}^* + \hat{q} \circ \hat{g}_i \circ \delta \hat{q}^* \\ &= \delta \hat{q} \circ \hat{q}^* \circ \hat{G}_i + \hat{G}_i \circ \hat{q} \circ \delta \hat{q}^* \\ &= \delta \hat{q} \circ \hat{q}^* \circ \hat{G}_i - \hat{G}_i \circ \delta \hat{q} \circ \hat{q}^*. \end{aligned}$$

In the above derivation, we take into account the variation of a conjugated quaternion as defined in Eq. (3),

$$\delta \hat{q}^* = -\hat{q}^* \circ \delta \hat{q} \circ \hat{q}^*. \tag{16}$$

Left multiplication leads to  $\hat{q} \circ \delta \hat{q}^* = -\delta \hat{q} \circ \hat{q}^*$ , which is a common property for all pure quaternions. Therefore, by using quaternion multiplication according to Eq. (2), we can write

$$\delta \hat{G}_i = 2\delta \hat{q} \circ \hat{q}^* \circ \hat{G}_i = \delta \hat{\vartheta} \circ \hat{G}_i, \tag{17}$$

where  $\delta \hat{\vartheta}$  denotes a non-unit pure quaternion  $2\delta \hat{q} \circ \hat{q}^*$ . It represents the variational part of a rotated vector.

### 2.4 Equilibrium and strain measures

It is convenient to express the equilibrium equations in the global frame,

$$\mathbf{n}_g(s) = -\mathbf{N}'_g(s), \tag{18}$$

$$\mathbf{m}_g(s) = -\mathbf{M}'_g(s) - \mathbf{r}'_g(s) \times \mathbf{N}_g(s). \tag{19}$$

Here,  $\mathbf{n}$  and  $\mathbf{m}$  are external distributed force and moment vectors per unit length of the undeformed configuration, and  $\mathbf{N}$  and  $\mathbf{M}$  are the stress resultant force and moment vectors, respectively.

A three-dimensional finite-strain beam theory introduces two strain vectors: a translational strain vector  $\boldsymbol{\gamma}$  and a rotational strain vector  $\boldsymbol{\kappa}$ . In the material frame description, the components of these vectors represent: extensional strain  $\boldsymbol{\gamma}_{G1}$ , shear strains  $\boldsymbol{\gamma}_{G2}$  and  $\boldsymbol{\gamma}_{G3}$ , torsional strain  $\boldsymbol{\kappa}_{G1}$  and bending strains  $\boldsymbol{\kappa}_{G2}$  and  $\boldsymbol{\kappa}_{G3}$ .

Following the approach of Reissner [11], the virtual work principle is applied,

$$\int_0^L (N_G \cdot \delta \boldsymbol{\gamma}_G + \mathbf{M}_G \cdot \delta \boldsymbol{\kappa}_G) ds = \int_0^L (\mathbf{n}_g \cdot \delta \mathbf{r}_g + \mathbf{m}_g \cdot \delta \boldsymbol{\vartheta}_g) ds + [\mathbf{F}_g \cdot \delta \mathbf{r}_g + \mathbf{P}_g \cdot \delta \boldsymbol{\vartheta}_g]_0^L. \tag{20}$$

Here, force and moment vectors  $N_G, \mathbf{M}_G$  and virtual strains  $\delta \boldsymbol{\gamma}_G, \delta \boldsymbol{\kappa}_G$  are expressed with respect to the local basis, while external distributed loads  $\mathbf{n}_g, \mathbf{m}_g$ , virtual displacements  $\delta \mathbf{r}_g$  and rotations  $\delta \boldsymbol{\vartheta}_g$ , and boundary point forces and moments  $\mathbf{F}_g(0), \mathbf{P}_g(0), \mathbf{F}_g(L)$  and  $\mathbf{P}_g(L)$  are written with respect to the global basis. The generalized virtual work principle can be expanded into four dimensions with a substitution of a rotational vector with rotational quaternion, as presented in the work by Zupan et al. [40]. After inserting equilibrium equations (18) and (19) into the principle of virtual work and following the calculus of variation, we obtain linearized kinematic relations between virtual strains, virtual displacements and virtual rotational quaternions. We write the result in quaternion form as follows:

$$\delta \hat{\boldsymbol{\gamma}}_G = \hat{q}^* \circ \delta \hat{r}'_g \circ \hat{q} + 2\hat{q}^* \circ (\hat{r}'_g \circ (\delta \hat{q} \circ \hat{q}^*)) \circ \hat{q}, \tag{21}$$

$$\delta \hat{\boldsymbol{\kappa}}_G = 2\hat{q}^* \circ (\delta \hat{q} \circ \hat{q}^*)' \circ \hat{q}. \tag{22}$$

For the integration of Eqs. (21) and (22), a special attention is needed. We recognize the term  $2\delta \hat{q} \circ \hat{q}^* = \delta \hat{\boldsymbol{\vartheta}}$  in Eq. (21) from Eq. (17). This means that  $\delta \hat{\boldsymbol{\gamma}}_G$  is a measure for the rate of change of vector  $\hat{q}^* \circ \hat{r}'_g \circ \hat{q}$  due to the variation of the rotational quaternion. We can write:

$$\hat{\boldsymbol{\gamma}}_G = \hat{q}^* \circ \hat{r}'_g \circ \hat{q} + \hat{c}_G. \tag{23}$$

With further application of quaternion algebra, Zupan et al. [23] provide the relationship between the curvature vector and the rotational quaternion:

$$\hat{\boldsymbol{\kappa}}_G = 2\hat{q}^* \circ \hat{q}' + \hat{d}_G, \tag{24}$$

where the unknown variational constants  $\hat{c}_G(s)$  and  $\hat{d}_G(s)$  are vector functions to be determined from the known strain and kinematic measures in the initial configuration of the beam. The initial curvature and twist along the length of the beam can be introduced through these constants, but they do not change throughout the loading process. In the initial state of the beam, its cross-sections are usually considered to be orthogonal to the centroid axis, i.e. orthogonal to the tangent vector  $d\mathbf{r}_g^0(s)/ds$ . If we further assume that the beam is initially undeformed, i.e. that the strains and rotations are zero:  $\hat{\boldsymbol{\gamma}}_G^0 \equiv \hat{0}, \hat{\boldsymbol{\kappa}}_G^0 \equiv \hat{0}$  and  $\hat{q} \equiv \hat{q}_0, [\hat{k}] = [1, 0, 0, 0]^T$ , the variational constants  $\hat{c}_G$  and  $\hat{d}_G$  are

$$\hat{c}_G = \hat{\boldsymbol{\gamma}}_G^0 - \hat{q}_0^* \circ \hat{r}'_g \circ \hat{q}_0 = -\hat{G}_1^0, \tag{25}$$

$$\hat{d}_G = \hat{\boldsymbol{\kappa}}_G^0 - 2\hat{q}_0^* \circ \hat{q}'_0 = -2\hat{q}_0^* \circ \hat{q}'_0. \tag{26}$$

If the beams are curved in the undeformed configuration, we can separate the influence of the initial geometry from the rotational deformations. Inserting Eq. (13) for the total rotation into Eq. (24) splits the total curvature into two parts: the rotational strain  $\hat{\boldsymbol{\kappa}}_G(\hat{k})$  and the initial curvature  $\hat{\boldsymbol{\kappa}}_G^0(\hat{q}_0)$ ,

$$\begin{aligned} \hat{\boldsymbol{\kappa}}_G(\hat{q}) &= 2\hat{q}_0^* \circ \hat{k}^* \circ (\hat{k} \circ \hat{q}_0)' + \hat{d}_G \\ &= 2\hat{q}_0^* \circ \hat{k}^* \circ \hat{k}' \circ \hat{q}_0 + 2\hat{q}_0^* \circ \hat{q}'_0 + \hat{d}_G \\ &= \hat{q}_0^* \circ \hat{\boldsymbol{\kappa}}_G(\hat{k}) \circ \hat{q}_0 + \hat{\boldsymbol{\kappa}}_G^0(\hat{q}_0) + \hat{d}_G \\ &= Q_0(\hat{q}_0)\hat{\boldsymbol{\kappa}}_G(\hat{k}). \end{aligned}$$

We can notice that the initial curvature  $\hat{\boldsymbol{\kappa}}_G^0(\hat{q}_0)$  vanishes when we add variational constant  $\hat{d}_G$ . The total curvature vector is simply obtained by multiplying initial rotation matrix and rotational strain. Therefore, the split of the total rotational quaternion (13) further simplifies the expressions.

Finally, we can write the curvature and translational strain vectors with respect to both bases by employing Eqs. (14) and (15):

$$\hat{\boldsymbol{\gamma}}_g = \hat{r}'_g - \hat{q} \circ \hat{G}_1 \circ \hat{q}^*, \tag{27}$$

$$\hat{\boldsymbol{\gamma}}_G = \hat{q}^* \circ \hat{r}'_g \circ \hat{q} - \hat{G}_1 \tag{28}$$

and

$$\hat{\boldsymbol{\kappa}}_g = 2\hat{k}' \circ \hat{k}^*, \tag{29}$$

$$\hat{\boldsymbol{\kappa}}_G = 2\hat{q}_0^* \circ \hat{k}^* \circ \hat{k}' \circ \hat{q}_0. \tag{30}$$

We will choose the strain vectors as the primary unknowns of the problem and assume them to be constant along the length of beam. For the reasons which will become evident later, we will express the translational strain vector in global basis and denote  $\hat{\boldsymbol{\gamma}}_g^{L/2}$ , while the rotational strain vector will be expressed in the local basis and denoted by  $\hat{\boldsymbol{\kappa}}_G^{L/2}$ . In accord with the discretization scheme that follows, they will be evaluated at the mid-length and are thus denoted with upper index  $L/2$ . After assuming constant strain measures, we can directly integrate kinematic equations (27) and (30) and express the position vector  $\hat{r}_g(s)$  and the relative rotational quaternion  $\hat{k}(s)$  with respect to translational strain and curvature:

$$\hat{r}_g(s) = \hat{r}_g(0) + \hat{\boldsymbol{\gamma}}_g^{L/2}s + \int_0^s Q(\tilde{s})\hat{G}_1(\tilde{s})d\tilde{s}, \tag{31}$$

$$\hat{k}(s) = \hat{k}(0) \circ \exp(Q_0(0)\hat{\boldsymbol{\kappa}}_G^{L/2}s/2). \tag{32}$$

Equation (32) is derived by following the work by Zupan et al. [39]. The above formulae determine the shape functions

of displacement and rotation field of our element. Note, that such an element gives exact results for constant strains.

### 2.5 Constitutive equations

Constitutive forces and moments are evaluated from a linear constitutive law as,

$$\hat{N}_G^C = C_N(\gamma_G, \kappa_G) = \hat{C}_{N_\gamma} \hat{\gamma}_G + \hat{C}_{N_\kappa} \hat{\kappa}_G, \tag{33}$$

$$\hat{M}_G^C = C_M(\gamma_G, \kappa_G) = \hat{C}_{M_\gamma} \hat{\gamma}_G + \hat{C}_{M_\kappa} \hat{\kappa}_G, \tag{34}$$

where the operators  $C_N(\gamma_G, \kappa_G)$  and  $C_M(\gamma_G, \kappa_G)$  are represented with the following  $4 \times 4$  matrices

$$[\hat{C}_{N_\gamma}] = \begin{bmatrix} 1 & 0 & 0 & 0 \\ 0 & EA & 0 & 0 \\ 0 & 0 & GA_s & 0 \\ 0 & 0 & 0 & GA_s \end{bmatrix}$$

and

$$[\hat{C}_{M_\kappa}] = \begin{bmatrix} 1 & 0 & 0 & 0 \\ 0 & GJ_1 & 0 & 0 \\ 0 & 0 & EJ_2 & 0 \\ 0 & 0 & 0 & EJ_3 \end{bmatrix}.$$

Young and shear moduli are here denoted by  $E$  and  $G$ , respectively,  $A$  is an area of the cross-section and  $A_s$  is the effective shear area, torsional moment of inertia is denoted with  $J_1$  and second moments of area about corresponding principal axes with  $J_2$  and  $J_3$ . In a more general case, where the beam axis does not pass through the centroid and shear center, off-diagonal terms, including deviatoric and static moment of area would appear in constitutive matrices. Note, that the accuracy of  $\hat{N}_G^C$  and  $\hat{M}_G^C$  is the same as that of the primary unknowns, which allows us to elegantly avoid the shear-locking (see also [25]).

From the equilibrium equations it is also suitable to express the resultant stresses in fixed basis, as follows:

$$\begin{aligned} \hat{N}_g^C &= \hat{q} \circ \hat{N}_G^C \circ \hat{q}^* = Q \hat{N}_G^C \\ &= Q \hat{C}_{N_\gamma} Q^T \hat{\gamma}_g + Q \hat{C}_{N_\kappa} \hat{\kappa}_G, \end{aligned} \tag{35}$$

$$\begin{aligned} \hat{M}_g^C &= \hat{q} \circ \hat{M}_G^C \circ \hat{q}^* = Q \hat{M}_G^C \\ &= Q \hat{C}_{M_\gamma} Q^T \hat{\gamma}_g + Q \hat{C}_{M_\kappa} \hat{\kappa}_G. \end{aligned} \tag{36}$$

### 2.6 Governing equations

External loads  $\hat{n}_g(s)$  and  $\hat{m}_g(s)$  are assumed to be known analytical functions of the arc-length parameter  $s$ . With this at hand, equilibrium Eqs. (18) and (19) can be directly integrated

$$\hat{N}_g(s) = \hat{N}_g(0) - \int_0^s \hat{n}_g(\tilde{s}) d\tilde{s}, \tag{37}$$

$$\hat{M}_g(s) = \hat{M}_g(0) - \int_0^s \hat{m}_g(\tilde{s}) d\tilde{s} - \int_0^s \hat{r}'_g(\tilde{s}) \times \hat{N}_g(\tilde{s}) d\tilde{s}. \tag{38}$$

Using a skew-symmetric operator  $As$  (see [41]), we replace a vector product with a matrix multiplication as

$$\mathbf{v} \times \mathbf{u} = As(\mathbf{v})\mathbf{u} = -As(\mathbf{u})\mathbf{v}, \tag{39}$$

$$[As(\mathbf{v})][\mathbf{u}] = \begin{bmatrix} 0 & -v_3 & v_2 \\ v_3 & 0 & -v_1 \\ -v_2 & v_1 & 0 \end{bmatrix} \begin{bmatrix} u_1 \\ u_2 \\ u_3 \end{bmatrix}, \tag{40}$$

and rewrite Eq. (19) accordingly,

$$\begin{aligned} \hat{M}_g(s) &= \hat{M}_g(0) + \int_0^s \left( As(\hat{N}_g(\tilde{s})) \hat{r}'_g(\tilde{s}) - \hat{m}_g(\tilde{s}) \right) d\tilde{s} \\ &= \hat{M}_g(0) + \int_0^s \left( As(\hat{N}_g(\tilde{s})) (\hat{\gamma}_g^{L/2} \right. \\ &\quad \left. + Q(\tilde{s}) \hat{G}_1(\tilde{s}) - \hat{m}_g(\tilde{s})) \right) d\tilde{s}. \end{aligned} \tag{41}$$

The set of governing equations consists of constitutive Eqs. (35), (36), equilibrium Eqs. (37), (41), kinematic Eqs. (31), (32) and boundary conditions. Constitutive relations are evaluated at the mid-point of the beam. To put the beam into physical space (three-dimensional Euclidean space  $\mathbb{R}^3$ ), we evaluate the kinematic equations at  $s = L$ , resulting in discrete relations between primary unknowns at  $s = 0$ ,  $s = L$  and  $s = L/2$ .

$$1 \hat{e} = \hat{N}_g^C(L/2) - \hat{N}_g(L/2) = \hat{0}, \tag{42}$$

$$2 \hat{e} = \hat{M}_g^C(L/2) - \hat{M}_g(L/2) = \hat{0}, \tag{43}$$

$$3 \hat{e} = \hat{r}_g^L - \hat{r}_g^0 - \hat{\gamma}_g^{L/2} L - \int_0^L Q(s) \hat{G}_1(s) ds = \hat{0}, \tag{44}$$

$$4 \hat{e} = \hat{k}^L - \phi_L(\hat{k}^0) \exp\left(\frac{L}{2} Q_0 \hat{k}_G^{L/2}\right) = \hat{0}, \tag{45}$$

$$5 \hat{e} = \hat{F}_g^0 + \hat{N}_g^0 = \hat{0}, \tag{46}$$

$$6 \hat{e} = \hat{P}_g^0 + \hat{M}_g^0 = \hat{0}, \tag{47}$$

$$7 \hat{e} = \hat{F}_g^L - \hat{N}_g(L) = \hat{0}, \tag{48}$$

$$8 \hat{e} = \hat{P}_g^L - \hat{M}_g(L) = \hat{0}. \tag{49}$$

Here,  $\hat{F}_g^0$  and  $\hat{F}_g^L$  denote external forces, while  $\hat{P}_g^0$  and  $\hat{P}_g^L$  denote external moments at the beginning and the end of the beam element. Constitutive and equilibrium equations are evaluated at the mid-length of the beam. In this way, the (left-right) orientation of the centroidal axis becomes irrelevant, resulting in orientation-independent finite elements that are symmetrical with respect to the mid-length point. Primary

variables of this formulation  $\hat{r}_g^0, \hat{r}_g^L, \hat{k}^0, \hat{k}^L, \hat{N}_g^0, \hat{M}_g^0, \hat{\gamma}_g^{L/2}$  and  $\hat{\kappa}_G^{L/2}$  are denoted with indices 0,  $L$  and  $L/2$  to determine their position on the beam with respect to the arc-length parameter  $s$  of the undeformed beam.

### 3 Numerical implementation

#### 3.1 Linearization

Before we linearize the system of non linear equations (42)–(49), it is suitable to prepare some terms first.

Variational form of Eqs. (14) and (15) is:

$$\begin{aligned} \delta Q \hat{a}_G &= \delta \hat{k} \circ \hat{k}^* \circ \hat{k} \circ \hat{q}_0 \circ \hat{a}_G \circ \hat{q}_0^* \circ \hat{k}^* \\ &\quad - \hat{k} \circ \hat{q}_0 \circ \hat{a}_G \circ \hat{q}_0^* \circ \hat{k}^* \circ \delta \hat{k} \circ \hat{k}^* \\ &= (\phi_R(Q_0 \hat{a}_G) - \phi_L(Q_0 \hat{a}_G)) \phi_R(\hat{k}^*) \delta \hat{k}, \end{aligned} \quad (50)$$

$$\begin{aligned} \delta Q^T \hat{a}_g &= -\hat{q}_0^* \circ \hat{k}^* \circ \delta \hat{k} \circ \hat{k}^* \circ \hat{a}_g \circ \hat{k} \circ \hat{q}_0 \\ &\quad + \hat{q}_0^* \circ \hat{k}^* \circ \hat{a}_g \circ \hat{k} \circ \hat{k}^* \circ \delta \hat{k} \circ \hat{q}_0 \\ &= Q_0^T (\phi_L(Z^T \hat{a}_g) - \phi_R(Z^T \hat{a}_g)) \phi_L(\hat{k}^*) \delta \hat{k}, \end{aligned} \quad (51)$$

where the variation of total rotation  $\delta \hat{q} = \delta \hat{k} \circ \hat{q}_0$  was taken into account.

Variational form of Eqs. (31) and (32) reads:

$$\begin{aligned} \delta \hat{r}_g(s) &= \delta \hat{r}_g^0 + s \delta \hat{\gamma}_g^{L/2} + \int_0^s \delta Q(\tilde{s}) \hat{G}_1(\tilde{s}) d\tilde{s} \\ &= \delta \hat{r}_g^0 + s \delta \hat{\gamma}_g^{L/2} + \int_0^s (\phi_R(Q(\tilde{s}) \hat{G}_1(\tilde{s})) \\ &\quad - \phi_L(Q(\tilde{s}) \hat{G}_1(\tilde{s}))) \phi_R(\hat{q}^*(\tilde{s})) \delta \hat{q}(\tilde{s}) d\tilde{s}, \end{aligned} \quad (52)$$

$$\begin{aligned} \delta \hat{k}(s) &= \delta \hat{k}^0 \circ \exp(Q_0 \hat{\kappa}_G^{L/2} s/2) \\ &\quad + \hat{k}^0 \circ \delta(\exp(Q_0 \hat{\kappa}_G^{L/2} s/2)) \\ &= \phi_R(\exp(Q_0 \hat{\kappa}_G^{L/2} s/2)) \delta \hat{k}^0 \\ &\quad + \phi_L(\hat{k}^0) T \delta \hat{\kappa}_G^{L/2}, \end{aligned} \quad (53)$$

where a variation of an exponential map is replaced by  $\delta(\exp(Q_0 \hat{\kappa}_G^{L/2} s/2)) = T(s) \delta \hat{\kappa}_G^{L/2}$ . The derivation of this relation is based on the directional derivative:

$$\begin{aligned} \delta(\exp(Q_0 \hat{\kappa}_G^{L/2} s/2)) &= \frac{d}{d\varepsilon} \left( \exp(Q_0(\hat{\kappa}_G^{L/2} + \varepsilon \delta \hat{\kappa}_G^{L/2}) s/2) \right) \Big|_{\varepsilon=0}, \end{aligned}$$

which after a short derivation leads to a compact formula

$$T = Q_0 a_0 I - a_0 K_0 s/2 + Q_0 a_1 K_1,$$

where  $I$  corresponds to a  $4 \times 4$  identity matrix, while  $K_0, K_1, a_0$  and  $a_1$  correspond to

$$\begin{aligned} [K_0] &= \begin{bmatrix} 0 & \kappa_{G1} & \kappa_{G2} & \kappa_{G3} \\ 0 & 0 & 0 & 0 \\ 0 & 0 & 0 & 0 \\ 0 & 0 & 0 & 0 \end{bmatrix}, \\ [K_1] &= \begin{bmatrix} 0 & 0 & 0 & 0 \\ 0 & \kappa_{G1} \kappa_{G1} & \kappa_{G1} \kappa_{G2} & \kappa_{G1} \kappa_{G3} \\ 0 & \kappa_{G2} \kappa_{G1} & \kappa_{G2} \kappa_{G2} & \kappa_{G2} \kappa_{G3} \\ 0 & \kappa_{G3} \kappa_{G1} & \kappa_{G3} \kappa_{G2} & \kappa_{G3} \kappa_{G3} \end{bmatrix}, \\ a_0 &= \kappa_G^{-1} \sin(\kappa_G s/2) \end{aligned}$$

and

$$a_1 = \kappa_G^{-2} \cos(\kappa_G s/2) s/2 - \kappa_G^{-3} \sin(\kappa_G s/2).$$

After inserting Eq. (53) into Eqs. (50) and (51), we see that every rotation or basis transformation depends upon the rotational quaternion at the beginning of the beam and its mid-length curvature. Therefore, the linearization of constitutive resultant forces and moments can be expressed with variations of strains and rotations as

$$\begin{aligned} \delta \hat{N}_g^C &= \delta Q \hat{N}_G^C + Q \delta \hat{N}_G^C \\ &= \delta Q \hat{N}_G^C + Q \hat{C}_{N_y} \delta Q^T \hat{\gamma}_g \\ &\quad + Q \hat{C}_{N_y} Q^T \delta \hat{\gamma}_g + Q \hat{C}_{N_k} \delta \hat{k}_G \\ &= (\phi_R(Q \hat{N}_G^C) - \phi_L(Q \hat{N}_G^C)) \phi_R(\hat{k}^*) \delta \hat{k} \\ &\quad + Q \hat{C}_{N_y} (\phi_L(Q^T \hat{\gamma}_g) - \phi_R(Q^T \hat{\gamma}_g)) \phi_L(\hat{k}^*) \delta \hat{k} \\ &\quad + Q \hat{C}_{N_y} Q^T \delta \hat{\gamma}_g + Q \hat{C}_{N_k} \delta \hat{k}_G, \end{aligned} \quad (54)$$

$$\begin{aligned} \delta \hat{M}_g^C &= \delta Q \hat{M}_G^C + Q \delta \hat{M}_G^C \\ &= \delta Q \hat{M}_G^C + Q \hat{C}_{M_y} \delta Q^T \hat{\gamma}_g \\ &\quad + Q \hat{C}_{M_y} Q^T \delta \hat{\gamma}_g + Q \hat{C}_{M_k} \delta \hat{k}_G \\ &= (\phi_R(Q \hat{M}_G^C) - \phi_L(Q \hat{M}_G^C)) \phi_R(\hat{k}^*) \delta \hat{k} \\ &\quad + Q \hat{C}_{M_y} (\phi_L(Q^T \hat{\gamma}_g) - \phi_R(Q^T \hat{\gamma}_g)) \phi_L(\hat{k}^*) \delta \hat{k} \\ &\quad + Q \hat{C}_{M_y} Q^T \delta \hat{\gamma}_g + Q \hat{C}_{M_k} \delta \hat{k}_G. \end{aligned} \quad (55)$$

Variations of equilibrium internal forces and moments, that follow from Eqs. (37) and (41), are:

$$\begin{aligned} \delta \hat{N}_g(s) &= \delta \hat{N}_g^0, \\ \delta \hat{M}_g(s) &= \delta \hat{M}_g^0 - \int_0^s (A_s(\hat{r}'_g(\tilde{s})) \delta \hat{N}_g(\tilde{s}) \\ &\quad - A_s(\hat{N}_g(\tilde{s})) \delta \hat{r}'_g(\tilde{s})) d\tilde{s} \\ &= \delta \hat{M}_g^0 - \int_0^s (A_s(\hat{\gamma}_g^{L/2} + Q(\tilde{s}) \hat{G}_1(\tilde{s})) \delta \hat{N}_g^0 \end{aligned} \quad (56)$$

$$-As(\hat{N}_g(\bar{s}))(\delta\hat{\gamma}_g + \delta Q(\bar{s})\hat{G}_1(\bar{s}))d\bar{s}. \quad (57)$$

After these preparations, the system of Eqs. (42)–(49) can be written in a compact linearized form as follows

$$\delta^1\hat{e} = \delta\hat{N}_g^C(L/2) - \delta\hat{N}_g(L/2), \quad (58)$$

$$\delta^2\hat{e} = \delta\hat{M}_g^C(L/2) - \delta\hat{M}_g(L/2), \quad (59)$$

$$\delta^3\hat{e} = \delta\hat{r}_g^L - \delta\hat{r}_g(L), \quad (60)$$

$$\delta^4\hat{e} = \delta\hat{k}^L - \delta\hat{k}(L), \quad (61)$$

$$\delta^5\hat{e} = \delta\hat{N}_g^0, \quad (62)$$

$$\delta^6\hat{e} = \delta\hat{M}_g^0, \quad (63)$$

$$\delta^7\hat{e} = -\delta\hat{N}_g^0, \quad (64)$$

$$\delta^8\hat{e} = -\delta\hat{M}_g(L). \quad (65)$$

### 3.2 Numerical solution procedure

With linearized equations at hand, we can construct a tangent stiffness matrix  $K^{[n]}$  and a residual  $f^{[n]}$  for the current configuration in iteration  $n$ . Let  $\delta y$  denote a vector of corrections of the primary unknowns:  $\delta\hat{r}_g^0$ ,  $\delta\hat{k}^0$ ,  $\delta\hat{r}_g^L$ ,  $\delta\hat{k}^L$ ,  $\delta\hat{N}_g^0$ ,  $\delta\hat{M}_g^0$ ,  $\delta\hat{\gamma}_g^{L/2}$  and  $\delta\hat{k}_G^{L/2}$ . Since our configuration space is a four-dimensional space of quaternions, the total number of degrees of freedom per each element is 26 (2 rotational quaternions and 6 pure quaternions). Corrections of the primary unknowns are obtained in each iteration as the solution of a system of linear equations  $K^{[n]}\delta y = -f^{[n]}$ .

Position vectors at boundaries of the element, internal forces, moments and translational strains are expressed in the fixed global basis. Therefore, updated values in new iteration  $n + 1$  are obtained by simply adding the corrections to the values at the current iteration  $n$ :

$$\hat{r}_g^{p[n+1]} = \delta\hat{r}_g^p + \hat{r}_g^{p[n]}, \quad (66)$$

$$\hat{N}_g^{0[n+1]} = \delta\hat{N}_g^0 + \hat{N}_g^{0[n]}, \quad (67)$$

$$\hat{M}_g^{0[n+1]} = \delta\hat{M}_g^0 + \hat{M}_g^{0[n]}, \quad (68)$$

$$\hat{\gamma}_g^{L/2[n+1]} = \delta\hat{\gamma}_g^{L/2} + \hat{\gamma}_g^{L/2[n]}, \quad (69)$$

where  $p \in \{0, L\}$ .

Note that due to the non-standard choice of the component form of the translational strain vector, the exactness of the update Eq. (69) needs some additional explanation. To prove Eq. (69) we first rearrange Eqs. (27) and (21) and insert them into the derivative of Eq. (66):

$$\begin{aligned} \delta\hat{r}_g' + \hat{r}_g'^{[n]} &= 2\delta\hat{q} \circ \hat{q}^* \circ \hat{r}_g' + \hat{q} \circ \delta\hat{\gamma}_G \circ \hat{q}^* \\ &\quad + \hat{q}^{[n]} \circ \hat{\gamma}_G^{[n]} \circ \hat{q}^{*[n]} + \hat{q}^{[n]} \circ \hat{G}_1 \circ \hat{q}^{*[n]} \\ &= 2\delta\hat{q} \circ \hat{q}^* \circ (\hat{q} \circ \hat{\gamma}_G \circ \hat{q}^* + \hat{q} \circ \hat{G}_1 \circ \hat{q}^*) \\ &\quad + \hat{q} \circ \delta\hat{\gamma}_G \circ \hat{q}^* + \hat{q}^{[n]} \circ \hat{\gamma}_G^{[n]} \circ \hat{q}^{*[n]} \\ &\quad + \hat{q}^{[n]} \circ \hat{G}_1 \circ \hat{q}^{*[n]}. \end{aligned} \quad (70)$$

Following the same procedure as for Eq. (17) we can replace the term  $\hat{q} \circ \delta\hat{\gamma}_G \circ \hat{q}^* + 2\delta\hat{q} \circ \hat{q}^* \circ \hat{q} \circ \hat{\gamma}_G \circ \hat{q}^*$  with  $\delta\hat{\gamma}_g$ . Since the vectors expressed in a fixed basis can be directly summed, the sum of the transformed cross-sectional normal vector  $\hat{q}^{[n]} \circ \hat{G}_1 \circ \hat{q}^{*[n]}$  and its variation is equal to the update of the same vector

$$\hat{q}^{[n]} \circ \hat{G}_1 \circ \hat{q}^{*[n]} + \delta(\hat{q}^{[n]} \circ \hat{G}_1 \circ \hat{q}^{*[n]}) = \hat{q}^{[n+1]} \circ \hat{G}_1 \circ \hat{q}^{*[n+1]}. \quad (71)$$

Inserting Eq. (71) into (70), leads to

$$\begin{aligned} \hat{r}_g'^{[n+1]} &= \hat{q}^{[n+1]} \circ \hat{\gamma}_G^{[n+1]} \circ \hat{q}^{*[n+1]} + \hat{q}^{[n+1]} \circ \hat{G}_1 \circ \hat{q}^{*[n+1]} \\ &= \delta\hat{\gamma}_g + \hat{q}^{[n]} \circ \hat{\gamma}_G^{[n]} \circ \hat{q}^{*[n]} + \hat{q}^{[n+1]} \circ \hat{G}_1 \circ \hat{q}^{*[n+1]} \end{aligned} \quad (72)$$

and considering the coordinate transformation, finally gives

$$\hat{\gamma}_g'^{[n+1]} = \delta\hat{\gamma}_g + \hat{\gamma}_g'^{[n]}. \quad (73)$$

On the other hand, rotational quaternions and curvature vectors are non-additive. Boundary nodal rotation corrections  $\delta\hat{k}^p$ , for  $p \in \{0, L\}$  at each element are expressed in the tangent space, which is not a space of unit quaternions. The tangential correction  $\delta\hat{k}$  is first mapped onto the space of unit quaternions:

$$\Delta\hat{k}^p = \cos|\delta\hat{k}^p \circ \hat{k}^{*p}| + \frac{[\delta\hat{k}^p \circ \hat{k}^{*p}]_{\mathbb{R}^3}}{|\delta\hat{k}^p \circ \hat{k}^{*p}|} \sin|\delta\hat{k}^p \circ \hat{k}^{*p}|, \quad (74)$$

and then multiplied to the current rotational quaternion

$$\hat{k}^{p[n+1]} = \Delta\hat{k}^p \circ \hat{k}^{p[n]}. \quad (75)$$

For further details see Zupan et al. [23].

Using Eq. (75) we can express the update of rotational strains. In the fixed basis, we have

$$\begin{aligned} \hat{k}_g'^{[n+1]}(\hat{k}^{[n+1]}) &= 2(\Delta\hat{k} \circ \hat{k}^{[n]})' \circ \hat{k}^{*[n]} \circ \Delta\hat{k}^* \\ &= 2\Delta\hat{k}' \circ \Delta\hat{k}^* + 2\Delta\hat{k} \circ \hat{k}'^{[n]} \circ \hat{k}^{*[n]} \circ \Delta\hat{k}^* \\ &= \Delta\hat{k}_g + \Delta\hat{k} \circ \hat{k}_g'^{[n]} \circ \Delta\hat{k}^*. \end{aligned} \quad (76)$$

Moreover, the transformation of the above expression into the local frame yields

$$\begin{aligned} \hat{\kappa}_{G^{[n+1]}}^{[n+1]} &= \hat{q}^{*[n+1]} \circ \Delta \hat{\kappa}_g \circ \hat{q}^{[n+1]} \\ &\quad + \hat{q}^{*[n+1]} \circ \Delta \hat{\kappa} \circ \hat{\kappa}_g^{[n]} \circ \Delta \hat{\kappa}^* \circ \hat{q}^{[n+1]} \\ &= \hat{q}^{*[n+1]} \circ \Delta \hat{\kappa}_g \circ \hat{q}^{[n+1]} + \hat{q}^{*[n]} \circ \hat{\kappa}_g^{[n]} \circ \hat{q}^{[n]} \\ &= \Delta \hat{\kappa}_{G^{[n+1]}} + \hat{\kappa}_{G^{[n]}}^{[n]}. \end{aligned} \tag{77}$$

### 4 Numerical examples

A thick cantilever beam, shear loaded double asymmetric tapered beam, a right-angle cantilever and a beam bent into a helical form are chosen to test our element. The numerical implementation of the code was done in Matlab [42]. The Gaussian quadrature rule is used to evaluate all integrals, in all our examples, 3 integration points were used. A tolerance  $10^{-8}$  for Euclidean norm of corrections was chosen to exit the iteration loop. The quadratic convergence was observed in all our examples, so we do not display it separately.

Our finite element has a total of 26 degrees of freedom. Therefore, a beam consisting of  $n_e$  elements has  $19n_e + 7$  degrees of freedom. The internal degrees of freedom, strain vectors  $\boldsymbol{\gamma}_g^{L/2}, \boldsymbol{\kappa}_G^{L/2}$  and boundary stress resultants  $\mathbf{N}_g^0, \mathbf{M}_g^0$  are not involved in the stiffness matrix construction process, as they are condensed at an element level. The matrix parts  $K_a, K_b, K_c$  and  $K_d$  and the vector parts  $f_a$  and  $f_c$  are extracted from the element stiffness matrix  $K_{el}$  and the element residual vector  $f_{el}$ ,

$$\begin{bmatrix} K_a & K_b \\ K_c & K_d \end{bmatrix} \begin{bmatrix} \delta y_{ext} \\ \delta y_{int} \end{bmatrix} = - \begin{bmatrix} f_a \\ f_c \end{bmatrix}. \tag{78}$$

The vector of corrections is divided into two parts; external  $[\delta y_{ext}] = [\delta \hat{r}_g^0, \delta \hat{k}^0, \delta \hat{r}_g^L, \delta \hat{k}^L]$  and internal  $[\delta y_{int}] = [\delta \hat{N}_g^0, \delta \hat{M}_g^0, \delta \hat{\gamma}_g^{L/2}, \delta \hat{\kappa}_G^{L/2}]$  degrees of freedom, which we calculate separately. All steps within an iteration loop are represented in pseudo-code 1.

The results are evaluated and compared in the form of a displacement vector and its components in the global basis  $[\mathbf{u}]_g = [u_1, u_2, u_3]^T$ . All four examples were also modeled in a commercial finite element software Ansys [43] using a two-node three-dimensional beam element B188.

#### 4.1 Thick cantilever beam subjected to free-end transverse force

A thick cantilever beam is subjected to a concentrated force at the free end, as shown in Fig. 2. The force vector is composed of two equal transverse components, which in matrix notation with respect to global basis  $g$  reads  $[\mathbf{F}(L)]_g = F[0, 1, 1]^T$ .

#### Pseudo-code 1 Iteration $n$

```

1: while norm( $f^{[n]}$ ) > tolerance do
2:   for element = 1 to  $n_e$  do
3:     evaluate  $f_{el}$ ;
4:     evaluate  $K_{el}$ ;
5:      $K_{cond} = K_c - K_d(K_b^{-1}K_a)$ ;
6:      $f_{cond} = f_c - K_d(K_b^{-1}f_a)$ ;
7:      $K_{const}(elDOF, elDOF) += K_{cond}$ ;
8:      $f_{const}(elDOF) += f_{cond}$ ;
9:   end for
10:  delete( $K_{const}(fixDOF, fixDOF)$ );
11:  delete( $f_{const}(fixDOF)$ );
12:   $\delta y_{ext} = -K_{const}^{-1}f_{const}$ ;
13:   $\delta y_{int} = K_b^{-1}(f_a - K_d\delta y_{ext})$ ;
14:  evaluate update procedure;
15: end while
    
```

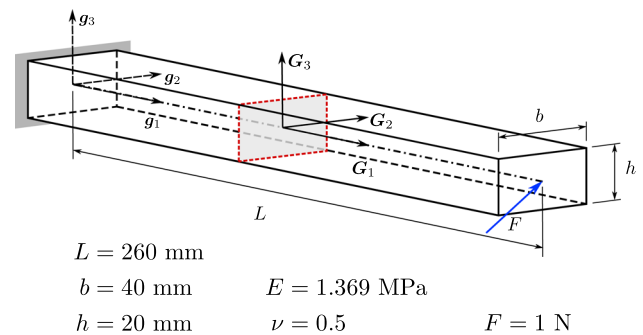


Fig. 2 A cantilever beam subjected to a concentrated force at the free end

We obtained these results by employing the presented model and also its modification, in which  $\boldsymbol{\gamma}_G$  (translational strain in local basis) is a primary unknown and a simple additive update of  $\boldsymbol{\gamma}_G$  is used. Note that a detailed derivation involving  $\boldsymbol{\gamma}_G$  (which is not given in this paper but was also fully integrated in our computer code), can be found e.g. in papers by Zupan et al. [23,24]. To distinguish between both formulations we will use labels  $\boldsymbol{\gamma}_g$  and  $\boldsymbol{\gamma}_G$ . The results are compared to the ones obtained by commercially available finite element B188 in Ansys and B31 element from Abaqus [44]. Even though it is a fairly simple example, different results can be observed for various finite element codes.

From the convergence analysis, shown in Table 1 we notice that all elements converge quite rapidly. Our formulations needed 6 iterations in one step to exit the loop, while B188 elements converged in two load steps. For a system of 50 or more elements, the difference between  $\boldsymbol{\gamma}_g$  and  $\boldsymbol{\gamma}_G$  elements is only present at the fifth decimal place. The absolute difference is approximately linear in logarithmic scale, which means that the error decreases exponentially with the number of elements. Figure 3 illustrates deformed configurations for 4 load steps to show the evolution of the deformation.

In order to observe the convergence rate of all quantities involved in both ( $\boldsymbol{\gamma}_g$  and  $\boldsymbol{\gamma}_G$ ) formulations, we present a convergence plot in Fig. 4. Relative error is calculated with

**Table 1** Free-end displacement vector components for different number of finite elements

	$n_e = 4$				$n_e = 10$			
	$\gamma_g$	$\gamma_G$	B188	B31	$\gamma_g$	$\gamma_G$	B188	B31
$u_1$	-39.9843	-39.9808	-41.5599	-42.0672	-40.7568	-40.7563	-42.4987	-42.5348
$u_2$	37.7694	37.7670	40.7048	41.1169	38.3319	38.3315	41.5264	41.6201
$u_3$	119.8349	119.8292	122.0192	122.928	121.1590	121.1580	122.5417	122.6921
	$n_e = 20$				$n_e = 50$			
	$\gamma_g$	$\gamma_G$	B188	B31	$\gamma_g$	$\gamma_G$	B188	B31
$u_1$	-40.8675	-40.8674	-42.8238	-42.6723	-40.8985	-40.8985	-42.6746	-42.6951
$u_2$	38.4128	38.4127	41.6851	41.7168	38.4354	38.4354	41.6876	41.7022
$u_3$	121.3469	121.3467	122.8596	122.652	121.3995	121.3994	122.6329	122.6430
	$n_e = 100$				$n_e = 200$			
	$\gamma_g$	$\gamma_G$	B188	B31	$\gamma_g$	$\gamma_G$	B188	B31
$u_1$	-40.9030	-40.9030	-42.6801	-42.6982	-40.9041	-40.9041	-42.6556	-42.6992
$u_2$	38.4387	38.4387	41.7072	41.7437	38.4395	38.4395	41.7324	41.7445
$u_3$	121.4070	121.4070	122.6341	122.6420	121.4089	121.4089	122.6164	122.6420

All results are in millimeters

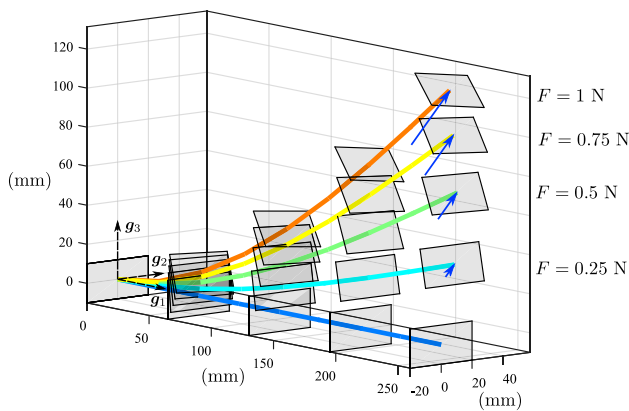


**Fig. 3** Deformed configurations of the cantilever beam subjected to transverse loads

respect to the value at the final (converged) iteration. After 6 iterations, all degrees of freedom reached their precision limits, while exhibiting quadratic convergence behaviour. Afterwards, there is no significant difference in the convergence of the two formulations.

### 4.2 Double asymmetric tapered beam

Although a thick beam theory accounts for shear deformation, numerical examples found in the literature are surprisingly often restricted to relatively small shear deformations. To fill this gap, we propose a double asymmetric tapered beam. The geometry, material properties, boundary conditions and loads are defined such that large shear deformation is observed (see Fig. 5 for details). The beam is clamped at one side while all rotation and longitudinal

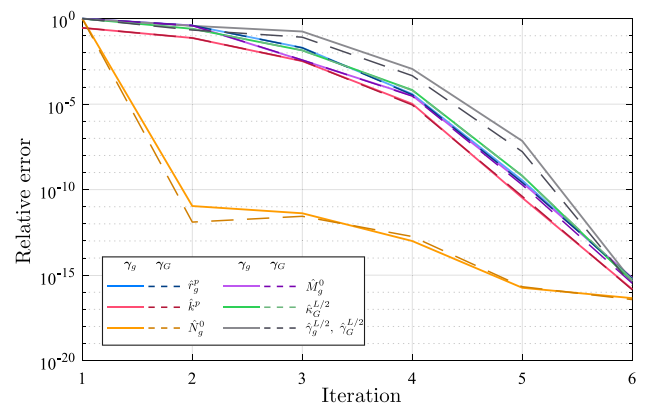


**Fig. 4** Relative error convergence evolution of distinct kinds of degrees of freedom. Solid line represents  $\gamma_g$  elements, while dashed line represents  $\gamma_G$  elements. Model is constructed with 50 elements

displacement components are restrained on the other side. The beam is subjected to a distributed load, defined with a vector  $n_g$ . For one half of the length of the beam, its value is  $[n(s)]_g = n_g[0, 1, 1]^T, 0 < s < L/2$  and for the other  $[n(s)]_g = n_g[0, -1, -1]^T, L/2 < s < L$ .

The height and width of the cross-section follow linear relations

$$B(s) = B_0 + \frac{B_L - B_0}{L}s \quad \text{and} \quad H(s) = H_0 + \frac{H_L - H_0}{L}s.$$

Results, given in Table 2, demonstrate the convergence of the problem for  $\gamma_g$  and  $\gamma_G$  elements, the B188 element from Ansys and the B31 element from Abaqus. All results are obtained with 1 load step.

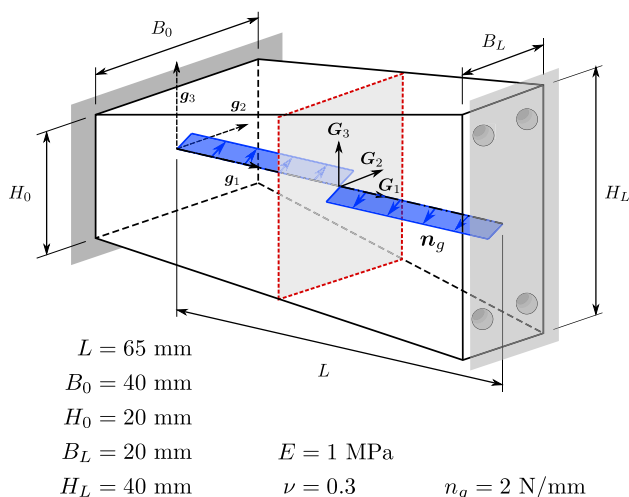


**Fig. 5** Geometrical model of a thick double asymmetric tapered beam subjected to distributed loads. One end is clamped, while the other is connected to a rigid panel through rollers restraining all rotations and axial displacement

Although the cross-sections are non-uniform, a symmetry of the problem can be observed from the results of Abaqus element B31 and our formulation. Results, obtained with commercial software Ansys converge to different values for displacement  $u_2(L)$  and  $u_3(L)$ , being 2.91% and 0.13% apart from our results. Convergence difficulties were noticed for  $\gamma_G$  formulation and the default loop termination criterion ( $10^{-8}$ ) was not reached. The solution (the norm of a residual vector) was trapped approximately between  $10^{-5}$  and  $10^{-6}$ . For this reason, the procedure with  $\gamma_G$  elements was stopped after 15 iterations of error norm fluctuation, while  $\gamma_g$  elements needed only 6 on average to converge altogether. Nonetheless, we notice that values of both,  $\gamma_g$  and  $\gamma_G$  elements yield very similar results and have better convergence rate than both commercial software elements.

**Table 2** Right-end displacement vector components for different finite elements

	$n_e = 4$				$n_e = 10$			
	$\gamma_g$	$\gamma_G$	B188	B31	$\gamma_g$	$\gamma_G$	B188	B31
$u_2$	15.79574	15.77233	15.12098	16.56631	15.85471	15.85122	15.34776	16.72924
$u_3$	15.79574	15.77233	15.36293	16.56631	15.85471	15.85122	15.75427	16.72924
	$n_e = 20$				$n_e = 50$			
	$\gamma_g$	$\gamma_G$	B188	B31	$\gamma_g$	$\gamma_G$	B188	B31
$u_2$	15.86215	15.86128	15.37514	16.75163	15.86418	15.86404	15.40146	16.78049
$u_3$	15.86215	15.86128	15.80817	16.75163	15.86418	15.86404	15.84070	16.78049
	$n_e = 100$				$n_e = 200$			
	$\gamma_g$	$\gamma_G$	B188	B31	$\gamma_g$	$\gamma_G$	B188	B31
$u_2$	15.86447	15.86444	15.40256	16.78132	15.86454	15.86453	15.40283	16.89724
$u_3$	15.86447	15.86444	15.84285	16.78132	15.86454	15.86453	15.84339	16.89724

All results are in millimeters

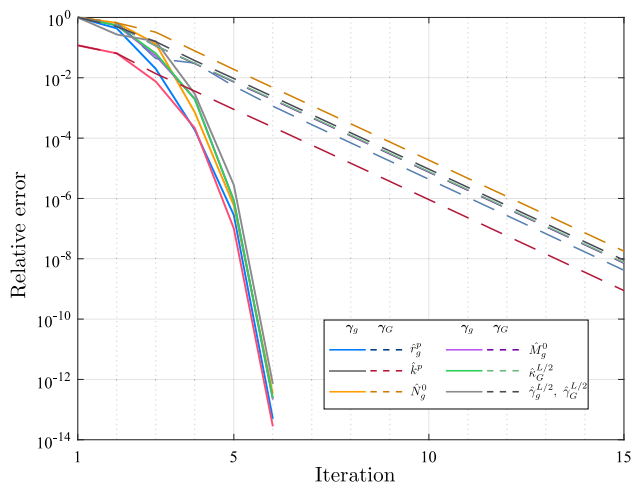


**Fig. 6** Relative error convergence evolution of primary unknowns. Solid line represents  $\gamma_g$  and dashed line  $\gamma_G$  elements. Model is constructed with 50 elements

Figure 6 depicts a relative error convergence plot for all primary unknowns of the  $\gamma_g$  and  $\gamma_G$  formulations. Note that  $\gamma_g$  elements reach lower precision limit within less iterations than  $\gamma_G$  elements.

When shear deformation is large, the error accumulates in every load step. Figure 7 portrays the difference between displacements calculated with both formulations,  $\gamma_G$  and  $\gamma_g$ , for various ratios of shear  $G$  and Young modulus  $E$ . As the load increases, the results grow apart, which is even more evident for cases with smaller rigidity in shear, i.e. where larger shear strains are developed. The displacement difference  $|u_{g2}(L) - u_{G3}(L)|$  decreases exponentially with the number of elements for all cases. The last case with extremely large shear modulus (grey curve) represents the shear rigid case which corresponds to the Euler-Bernoulli hypothesis on perpendicular cross-sections. Even in this case, the differences are still present.

Figure 8 depicts shear and bending strain for every element. Given that the norm of the curvature vector is substantially smaller than that of the translational strain vector, we can conclude that this problem is governed mainly by shear deformation (see the top right inset on both figures).

### 4.3 L-shaped cantilever beam

A beam with right angle between its segments of equal length is often studied in the literature [17,25,45]. Due to its geometry it is suitable for tests of beam formulations on torsion-bending coupling. With very slender segments ( $h/b = 1/50$ ), instabilities can occur during specific load-

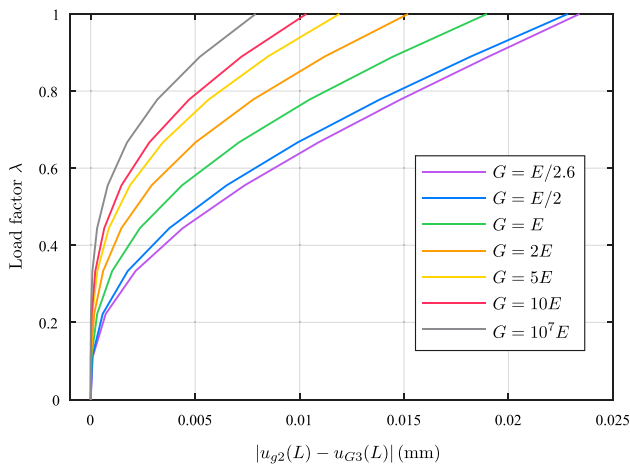
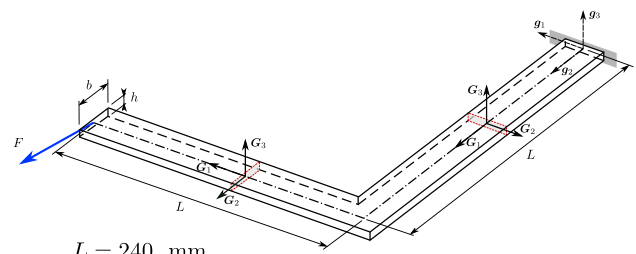
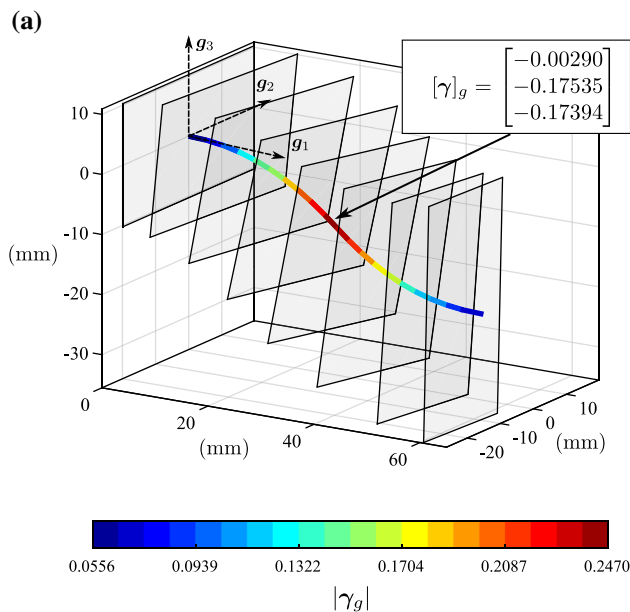


Fig. 7 Displacement difference for various shear moduli. We use 4 elements and 10 load steps



$L = 240 \text{ mm}$   
 $b = 30 \text{ mm}$        $E = 71240 \text{ MPa}$   
 $h = 0.6 \text{ mm}$        $\nu = 0.31$        $F = 1.9 \text{ N}$

Fig. 9 Schematic of a right-angle cantilever beam

ings. Figure 9 illustrates one such case, in which one end is fixed and the other is subjected to a force acting in the  $g_1$ - $g_2$ -plane. We also apply an out-of-plane perturbation force in the direction of the unit vector  $g_3$ . Hence, the matrix form of the force vector is  $[F(2L)]_g = F[0, 1, 0.001]^T$ . Geometrical and material properties given in the Fig. 9 are taken from Ref. [17].

Results presented in Fig. 10 are obtained with 10 elements (197 degrees of freedom) and 100 load steps. We compared them with the results from Smolenski [17] (20 two-node elements) and Zupan and Saje [25] (12 elements with 5 interpolation points; 510 degrees of freedom). An excellent agreement can be observed between our results and the results of these authors. In this case, both elements, based on  $\gamma_g$  and  $\kappa_G$  converge and yield practically the same result, since there is no substantial shear deformation, as shown in Fig. 11.

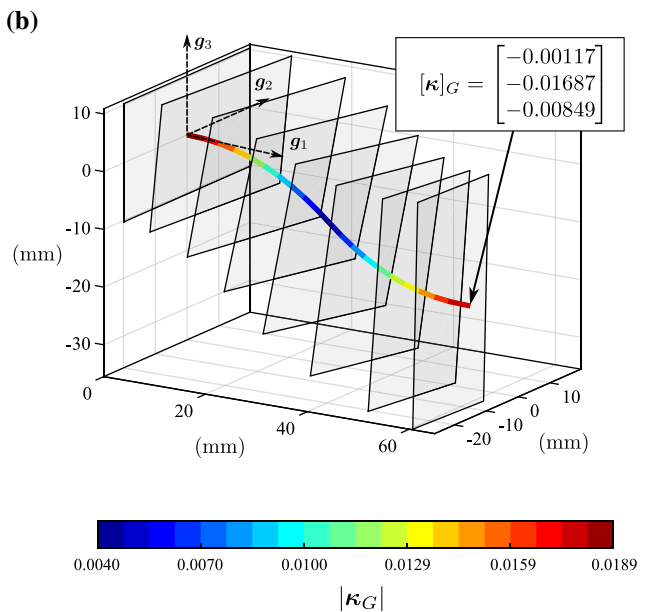
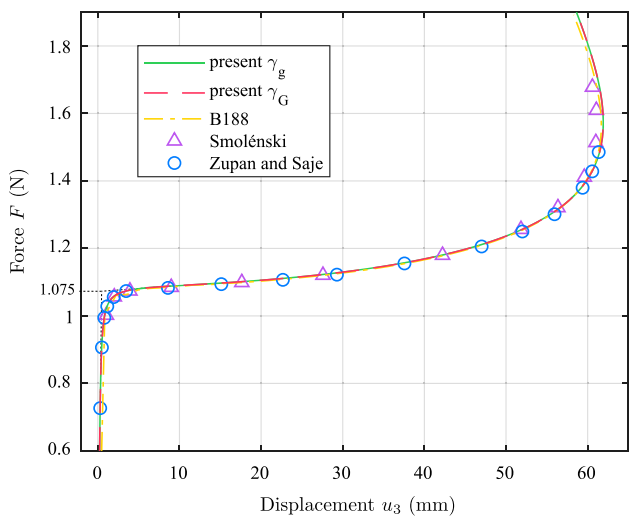


Fig. 8 Deformed configuration for  $\lambda = 1$  and  $G = E/2.6$ . Every element has the color corresponding to the Euclidean norm of **a** translational strain vector and **b** rotational strain vector

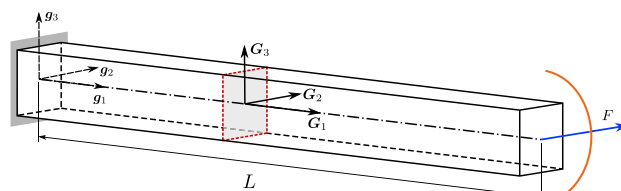


**Fig. 10** Lateral post-buckling region of a right angle beam subjected to an in-plane load

### 4.4 Beam bent into a helical form

An example, introduced by Ibrahimbegović [29] is often used to illustrate element’s ability to withstand large rotations. A cantilever beam is subjected to a concentrated force  $F$  and a bending moment  $M$  at the free end, as shown in Fig. 12. With moment  $M$  acting alone, the beam would bend into a circular shape with several revolutions in  $g_1$ – $g_3$ -plane, whereas a simultaneous action of force  $F$  and bending moment  $M$  produces a helical shape.

To test the convergence of finite elements, we vary the number of elements and compare displacements  $u_2$  for  $F = 50$  and  $M = 200\pi$ , see Table 3 for both  $\gamma_g$  and  $\gamma_G$  formula-



$$L = 10 \quad GA_2 = GA_3 = EA = 10^4 \quad M = 200\pi$$

$$EJ_2 = EJ_3 = GJ_1 = 10^2 \quad F = 50$$

**Fig. 12** A cantilever beam subjected to an end force and moment

tions. End force and moment are controlled by a load factor  $\lambda$ , increasing incrementally from 0 to 1 in 200 steps.

During loading, the height of such composed helix oscillates around zero value. Interestingly, the shape obtained in the final load step lies on the negative side of  $g_1$ – $g_3$ -plane. This effect is visible on the out-of-plane displacement  $u_2$  diagram in Fig. 13a.

Figure 13b presents a plot of displacement  $u_2$  versus load factor  $\lambda$ . Results of both element types coincide with the ones found in [23,24,29]. Our construction with 79 elements (1508 degrees of freedom) is in very good agreement with result from [25], which was obtained with 25 elements with 8 interpolation points (1506 degrees of freedom).

Since the beam in this case is mainly undergoing bending deformations, the differences between formulations are negligible. With the norm of translational strain vectors being relatively small, so is the error of the update. On average, one additional iteration is needed to reach the convergence criteria. Increasing the number of elements, their length becomes smaller and thus the difference in rotations between loading steps leads to better results. For example, Češarek et al. [24]

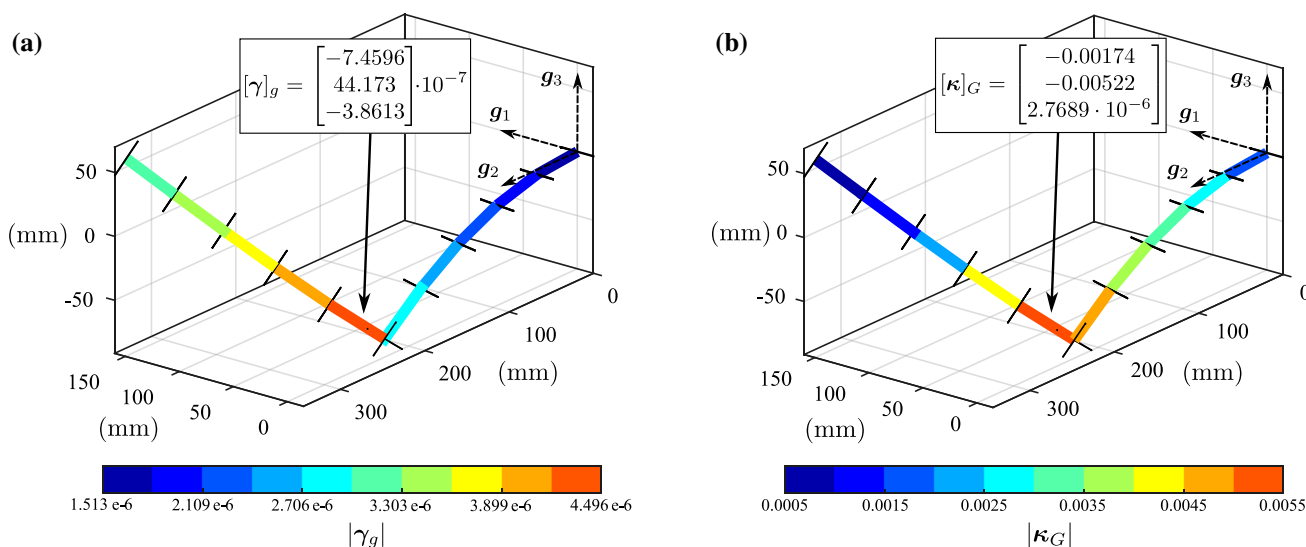


**Fig. 11** Deformed axis and rotated cross-sections for  $F = 1.9$  N where every element has the color corresponding to the Euclidean norm of **a** translational strain vector and **b** bending strain vector

**Table 3** Free-end displacement vector components for different number of elements

	$n_e = 50$		$n_e = 79$		$n_e = 100$	
	$\gamma_g$	$\gamma_G$	$\gamma_g$	$\gamma_G$	$\gamma_g$	$\gamma_G$
$u_1$	-9.982863	-9.983047	-9.99502	-9.995034	-9.995140	-9.995147
$u_2$	-0.089889	-0.090060	-0.083702	-0.083703	-0.080564	-0.080564
$u_3$	-0.002437	-0.002397	-0.000090	-0.000091	-0.000075	-0.000075
	$n_e = 200$		$n_e = 500$		$n_e = 1000$	
	$\gamma_g$	$\gamma_G$	$\gamma_g$	$\gamma_G$	$\gamma_g$	$\gamma_G$
$u_1$	-9.995181	-9.995183	-9.995194	-9.995194	-9.995196	-9.995196
$u_2$	-0.077480	-0.077480	-0.076608	-0.076608	-0.076483	-0.076483
$u_3$	-0.000073	-0.000073	-0.000073	-0.000073	-0.000073	-0.000073

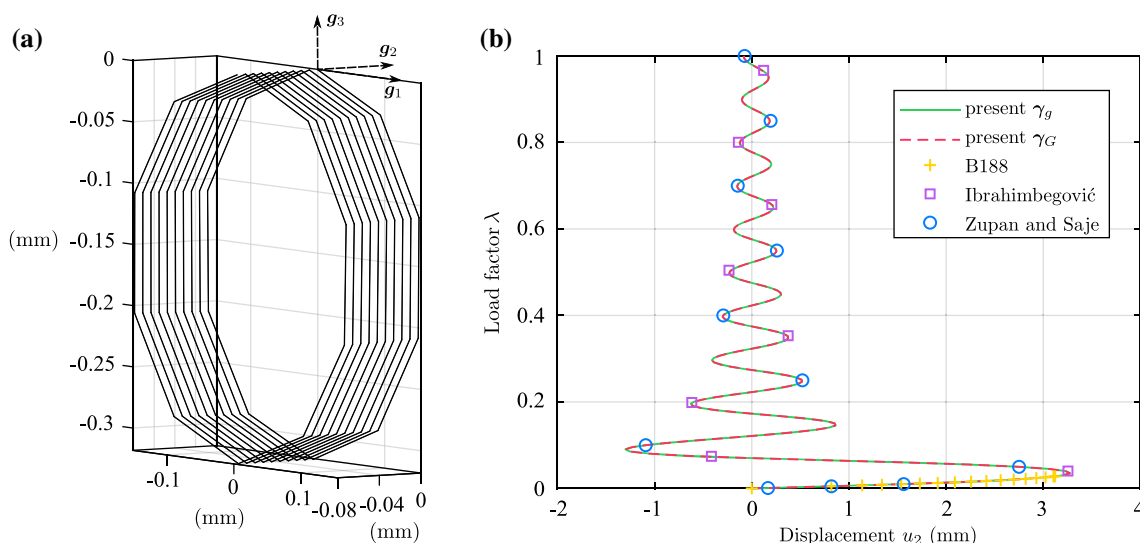


**Fig. 13** **a** Deformed configuration with 100 elements and **b** free end displacements  $u_2$

used 1000 load steps in finite element model composed of 200 constant strain elements, with translational strain expressed in local basis. Failure of commercial software finite elements to withstand large rotations was also reported in [24].

### 5 Conclusions

The present finite element formulation is based on a geometrically exact beam theory. In the derivation of our computational model, the emphasis is given to consistency and mathematical accuracy, which inherently results in a numerically stable formulation. Spatial rotations of cross-sections are parametrized using quaternion algebra in order to provide a singularity-free model, capable of describing large rotations. We choose strain measures as the primary unknowns and assume them to be constant along the length of an element. This is the only approximation regarding the derivation of governing equations. The choice of component description for the strain vector is supported by mathematical

argument on accurate updating procedure given in Sec. 3.2. The strain measures are now in fully consistent relationship with the current configuration, regardless the magnitude of strains, rotations and displacements. Linearization process is obtained within variational framework, while the implementation into the finite element model involves numerical integration (we applied Gaussian quadrature rule).

In the present model, the interpolation and collocation points coincide, thus we avoid the interpolation error. The only way to obtain more accurate results is by employing more elements in the model. Due to our efficient formulation, this process is not computationally demanding. The performance of the numerical model is tested on one custom and three standard numerical examples found in literature. We showed that even small number of elements yields satisfactory results when compared to other beam finite element formulations.

The update of translational strains can be a source of error in strain based formulations. Compared to the models where strains are updated in local basis our approach is consis-

tent with the configuration space. The differences are more evident for cases with large shear deformation. This effect is often overlooked in the literature, since vast number of the beam finite element numerical examples undergo rather small shear strains. For this reason, we devised an example of shear loaded double asymmetric tapered beam. In this case, shear deformation is characteristically larger than bending deformation, which consequently results in convergence difficulties for the elements with inconsistent update of translational strains. Although the difference in results reduces exponentially with the number of elements used, the present approach requires less iterations for the same accuracy.

**Acknowledgements** This work was supported by the Slovenian Research Agency through Grants P2-0263 and J2-8170. The support is gratefully acknowledged.

## References

- Hover FS (1997) Simulation of stiff massless tethers. *Ocean Eng* 24(8):765–783
- Nazmy AS, Abdel-Ghaffar AM (1990) Three-dimensional nonlinear static analysis of cable-stayed bridges. *Comput Struct* 34(2):257–271
- Coleman BD, Swigon D (2000) Theory of supercoiled elastic rings with self-contact and its application to DNA plasmids. *J Elast* 60(3):173–221
- Nakano A (1999) A rigid-body-based multiple time scale molecular dynamics simulation of nanophase materials. *Int J High Perform Comput* 13(2):154–162
- Spillman J, Teschner M (2008) Cosserat nets. *IEEE Trans Vis Comput Graph* 15(2):325–338
- Gilles B, Bousquet G, Faure F, Pai DK (2011) Frame-based elastic models. *ACM Trans Graph* 30(2):15:1–15:12
- Horn BKP (1987) Closed-form solution of absolute orientation using unit quaternions. *J Opt Soc Am A* 4(4):629–642
- Trivedi D, Lotfi A, Rahn CD (2008) Geometrically exact models for soft robotic manipulators. *IEEE Trans Robot* 24(4):773–780
- Reissner E (1972) On one-dimensional finite-strain beam theory: the plane problem. *Z Angew Math Phys* 23(5):795–804
- Antman SS (2005) *Nonlinear problems of elasticity*. Springer, New York
- Reissner E (1981) On finite deformations of space-curved beams. *Z Angew Math Phys* 32(6):734–744
- Simo JC (1985) A finite strain beam formulation. The three-dimensional dynamic problem. Part I. *Comput Method Appl Mech* 49(1):55–70
- Simo JC, Vu-Quoc L (1986) A three-dimensional finite-strain rod model. Part II: computational aspects. *Comput Method Appl Mech* 58(1):79–116
- Cardona A, Géradin M (1988) A beam finite element non-linear theory with finite rotations. *Int J Numer Methods Eng* 26(11):2403–2438
- Ibrahimbegović A (1995) On finite element implementation of geometrically nonlinear Reissner's beam theory: three-dimensional curved beam elements. *Comput Methods Appl Mech* 22(1–2):11–26
- Jelenić G, Saje M (1995) A kinematically exact space finite strain beam model—finite element formulation by generalized virtual work principle. *Comput Methods Appl Mech* 120(1–2):131–161
- Smoleński WM (1999) Statically and kinematically exact nonlinear theory of rods and its numerical verification. *Comput Methods Appl Mech* 178(1–2):89–113
- Argyris J (1982) An excursion into large rotations. *Comput Methods Appl Mech* 32(1–3):85–155
- Argyris J, Poterasu VF (1993) Large rotations revisited application of Lie algebra. *Comput Methods Appl Mech* 103(1–2):11–42
- Géradin M, Rixen D (1995) Parametrization of finite rotations in computational dynamics: a review. *Revue Européenne des Eléments Finis* 4(5–6):497–553
- Spring KW (1986) Euler parameters and the use of quaternion algebra in the manipulation of finite rotations: a review. *Mech Mach Theory* 21(5):365–373
- Atluri SN, Cazzani A (1995) Rotations in computational solid mechanics. *Arch Comput Methods Eng* 2(1):49–138
- Zupan E, Saje M, Zupan D (2009) The quaternion-based three-dimensional beam theory. *Comput Methods Appl Mech* 198(49–52):3944–3956
- Češarek P, Saje M, Zupan D (2012) Kinematically exact curved and twisted strain-based beam. *Int J Solids Struct* 49(13):1802–1817
- Zupan D, Saje M (2003) Finite-element formulation of geometrically exact three-dimensional beam theories based on interpolation of strain measures. *Int J Solids Struct* 192(49–50):5209–5248
- Stuelpnagel J (1964) On the parametrization of the three-dimensional rotation group. *SIAM Rev* 6(4):422–430
- Pimenta PM, Campello EMB, Wriggers P (2008) An exact conserving algorithm for nonlinear dynamics with rotational DOFs and general hyperelasticity. Part I: rods. *Comput Mech* 42(5):715–732
- Neto AG, Martins CA, Pimenta PM (2014) Static analysis of offshore risers with a geometrically-exact 3D beam model subjected to unilateral contact. *Comput Mech* 53(1):125–145
- Ibrahimbegović A (1997) On the choice of finite rotation parameters. *Comput Methods Appl Mech* 149(1–4):49–71
- Crisfield MA, Jelenić G (1999) Objectivity of strain measures in the geometrically exact three-dimensional beam theory and its finite-element implementation. *Proc Roy Soc Lond A Math* 455(1–4):1125–1147
- Battini JM, Pacoste C (2002) Co-rotational beam elements with warping effects in instability problems. *Comput Methods Appl Mech* 191(17–18):1755–1789
- McRobie FA, Lasenby J (1999) Simo–Vu Quoc rods using Clifford algebra. *Int J Numer Methods Eng* 45(4):377–398
- Zupan E, Saje M, Zupan D (2013) Dynamics of spatial beams in quaternion description based on the Newmark integration scheme. *Comput Mech* 51(1):47–64
- Zupan E, Zupan D (2016) Velocity-based approach in non-linear dynamics of three-dimensional beams with enforced kinematic compatibility. *Comput Methods Appl Mech* 310:406–428
- Zupan E, Zupan D (2019) On conservation of energy and kinematic compatibility in dynamics of nonlinear velocity-based three-dimensional beams. *Nonlinear Dyn* 95(2):1379–1394
- Tabarrok B, Farshad M, Yi H (1988) Finite element formulation of spatially curved and twisted rods. *Comput Methods Appl Mech* 70(3):275–299
- Zupan D, Saje M (2006) The linearized three-dimensional beam theory of naturally curved and twisted beams: the strain vectors formulation. *Comput Methods Appl Mech* 195(33–36):4557–4578
- Ward JP (2012) *Quaternions and Cayley numbers: algebra and applications*. Springer, Berlin
- Zupan E, Zupan D (2014) On higher order integration of angular velocities using quaternions. *Mech Res Commun* 55:77–85
- Zupan E, Saje M, Zupan D (2013) On a virtual work consistent three-dimensional Reissner–Simo beam formulation using the quaternion algebra. *Acta Mech* 224(8):1709–1729
- Room TG (1952) The composition of rotations in Euclidean three-space. *Am Math Mon* 59(10):688–692

42. The Mathworks, Inc (2019) MATLAB version 9.6.0.1150989 (R2019a). Natick, Massachusetts
43. ANSYS, Inc. (2019) Academic research mechanical, release R2 2019. Help system, element reference
44. Dassault Systèmes Simulia Corp. (2019) ABAQUS documentation 6.13, Providence, RI, USA
45. Ibrahimbegović A, Taylor RL (2002) On the role of frame-invariance in structural mechanics models at finite rotations. *Comput Methods Appl Mech* 191(45):5159–5176

**Publisher's Note** Springer Nature remains neutral with regard to jurisdictional claims in published maps and institutional affiliations.